Article

Discovery Medicine 2026; 38(210): 2283–2299
https://doi.org/10.24976/Discov.Med.202638210.179

The Impact of Poly(ADP-ribose) Polymerase 1 on the Sensitivity of *Breast Cancer Type 1/2 Susceptibility* Wild-Type Ovarian Cancer Cells to Niraparib

Sijia Cheng[1,2,3,†], Yunzhi Ling[3,4,†], Jiayi Li[3,5], Jiaru Luo[3], Dan Zhou[1], Tianle Mao[1,3,6], Tingting Luo[3], Yanyang Tu[3], Jinlin Du[5], Minghui Zhou[1], Qingsong Qin[2,*], Yanqin Ji[1,*]

[1]Department of Gynecology, Huizhou Central People's Hospital, 516001 Huizhou, Guangdong, China
[2]Laboratory of Human Virology and Oncology, Shantou University Medical College, 515041 Shantou, Guangdong, China
[3]Science Research Center, Huizhou Central People's Hospital, 516001 Huizhou, Guangdong, China
[4]Department of Dermatology, Shenzhen People's Hospital (The First Affiliated Hospital, Southern University of Science and Technology; The Second Clinical Medical College, Jinan University), 518020 Shenzhen, Guangdong, China
[5]Department of Epidemiology and Statistics, School of Public Health, Guangdong Medical University, 523808 Dongguan, Guangdong, China
[6]The First School of Clinical Medicine, Guangdong Medical University, 524023 Zhanjiang, Guangdong, China
*Correspondence: qsqin@stu.edu.cn (Qingsong Qin); yqjihzch@163.com (Yanqin Ji)
[†]These authors contributed equally.
Submitted: 16 April 2026 Revised: 30 April 2026 Accepted: 18 May 2026 Published: 23 July 2026

Background: The Poly(ADP-ribose) polymerase (PARP) inhibitor niraparib improves survival in ovarian cancer, but its long-term efficacy was limited by acquired resistance. This study aimed to identify the key mechanism underlying acquired niraparib resistance in breast cancer type 1/2 susceptibility (*BRCA1/2*) wild-type ovarian cancer.

Methods: A stable niraparib-resistant cell line was generated by continuous drug exposure for six months (SKOV3_Nira_6M). Transcriptomic profiling (RNA-seq) and Western blot analysis were used to identify key changes in gene and protein expression. Functional roles were assessed by knocking down *PARP1* in parental cells and re-expressing it in resistant cells. Drug sensitivity was measured by cell counting kit-8 assay. Cell viability, proliferation, and apoptosis were evaluated using crystal violet staining, 5-ethynyl-2′-deoxyuridine (EdU) assay, and flow cytometry, respectively. *In vivo* validation was performed using subcutaneous xenograft models in nude mice established with doxycycline-inducible PARP1-knockdown (SKOV3) or *PARP1*-overexpressing (SKOV3_Nira_6M) stable cell lines.

Results: Transcriptomic and protein-level analyses consistently demonstrated a specific and significant downregulation of *PARP1* in resistant cells. Knocking down *PARP1* in parental SKOV3 cells induced resistance to niraparib, manifested as significantly enhanced cell viability and proliferation, reduced apoptosis, and diminished tumor growth inhibition by niraparib in nude mouse models. Conversely, overexpressing *PARP1* in the resistant SKOV3_Nira_6M cells partially restored sensitivity to niraparib, enhancing its cytotoxicity *in vitro* by inhibiting cell viability and proliferation and promoting apoptosis, while augmenting its inhibitory effect on tumor growth *in vivo*.

Conclusion: Our findings establish that downregulation of the drug target *PARP1* is a key driver of acquired niraparib resistance in *BRCA1/2* wild-type ovarian cancer, providing new mechanistic insight and identifying a potential target for overcoming clinical resistance.

Keywords: ovarian cancer; Poly(ADP-ribose) polymerase 1; PARP inhibitor resistance; niraparib

Introduction

The therapeutic landscape of ovarian carcinoma (OC) has been transformed by the emergence of Poly(ADP-ribose) polymerase (PARP) inhibitors [1]. These agents offer considerable survival advantages to patients with homologous recombination deficiency (HRD), especially those harboring pathogenic breast cancer type 1/2 susceptibility (*BRCA1/2*) mutations, via a synthetic lethality mechanism [2,3]. Niraparib, a potent and selective PARP1/2 inhibitor, is currently extensively employed in clinical settings. Key phase III clinical trials, like PRIMA, have shown that niraparib as first--line maintenance therapy notably enhances progression-free survival (PFS) in patients with advanced ovarian cancer, and this benefit extends to those with homologous recombination proficiency (HRp) or *BRCA1/2* wild-type (BRCAwt) status [4,5,6]. Nevertheless, the magnitude of clinical benefit in BRCAwt patients remains substantially more limited than that observed in patients with BRCA mutations, with only a moderate improvement in median PFS [7]. Real-world studies further corroborate the survival benefit of niraparib as second-

line maintenance therapy in BRCAwt patients [8]. However, these observations also emphasize that primary and acquired resistance remain the chief therapeutic obstacles in this large patient population, which accounts for approximately 75% of ovarian cancer cases [9,10]. Hence, systematically clarifying the mechanisms underlying niraparib resistance in BRCAwt ovarian cancer is not only an urgent clinical requirement to surmount current therapeutic limitations and expand the beneficiary population, but also a fundamental scientific issue for understanding the adaptive evolution of tumor cells under the selective pressure of targeted therapy.

The emergence of resistance is a multifactorial and dynamic process. The known mechanisms include the restoration of homologous recombination repair (e.g., BRCA reversion mutations), the enhancement of replication fork stability, the upregulation of drug efflux pumps (e.g., *ATP binding cassette subfamily B member 1* (*ABCB1*)), and the activation of alternative DNA repair pathways [11]. Notably, the expression and functional status of the PARP family proteins, which are direct targets of PARP inhibitors, are critical determinants of efficacy and resistance [12,13,14]. *PARP1* is the most predominant and extensively studied member of the PARP family, accounting for over 90% of cellular PARylation activity and serving as the core molecular target for all clinically used PARP inhibitors, including niraparib. Studies indicate that any factor affecting *PARP1* function or expression can lead to the failure or resistance of PARP inhibitor treatment [14]. Specifically, the downregulation of *PARP1* expression directly reduces the availability of the drug target, thereby contributing to primary resistance [11,15]. Moreover, mutations in specific domains of the PARP1 protein (e.g., the DNA-binding zinc finger domains) may hinder its binding to inhibitors, resulting in acquired resistance [16]. Recent research has also uncovered novel mechanisms by which *PARP1* drives acquired resistance through its transcriptional regulatory functions, such as activating the *disruptor of telomeric silencing 1-like* (*DOT1L*)-*phospholipase C gamma 2* (*PLCG2*)/*ABCB1* axis [13]. However, whether *PARP1* downregulation directly drives niraparib resistance in the BRCAwt context, as well as its exact molecular mechanism and role in transcriptional reprogramming of resistant cells, remains unknown.

Transcriptome sequencing technology provides an unbiased, global perspective to explore this complex process. It reveals a comprehensive view of dynamic gene expression profiles in tumor cells under drug pressure, moving beyond hypothesis-driven investigations of known pathways and providing the potential to discover novel key drivers and signaling networks underlying resistance. Based on this, the present study aims to systematically dissect the function and mechanism of *PARP1* in niraparib resistance in BRCAwt ovarian cancer through a multi-level integrated strategy. We established a niraparib-resistant cell model via long-term drug exposure and performed transcriptomic sequencing to identify consistently differentially expressed genes during the resistance evolution, with a focus on DNA damage response pathways, particularly PARP family members (*PARP1*, *PARP2*, *PARP3*). Molecular docking simulations were employed to preliminarily analyze potential changes in the interaction patterns between niraparib and PARP proteins at different expression levels from a structural perspective. Subsequently, *PARP1* was knocked down in parental cells to mimic the resistant phenotype, assessing its negative impact on niraparib sensitivity, cell viability, and clonogenic ability. Conversely, *PARP1* was re-overexpressed in the established resistant cells to determine whether it could reverse resistance and restore niraparib sensitivity. Finally, a nude mouse subcutaneous xenograft model was used to confirm the substantial regulatory effect of *PARP1* expression levels on the tumor-suppressive efficacy of niraparib *in vivo*.

This research endeavors to clarify how "*PARP1* downregulation" serves as a molecular hub, integrating and propelling a series of resistant phenotypes, ranging from protein-drug interactions and cellular functions to animal model phenotypes. The objective is to offer a mechanism-based elucidation for niraparib resistance in BRCAwt ovarian cancer, based on systems biology discoveries and validated through functional assays. Consequently, it lays a crucial theoretical and experimental foundation for the future development of combination strategies aimed at reversing resistance and accomplishing precise sensitization.

Materials and Methods

Acquisition and Culture of Ovarian Cancer Cells

SKOV3 cells (#SK-OV-2, Guangzhou Xinyuan Biotechnology Co., Ltd., Guangzhou, China) were cultured in McCoy's 5A medium (#Bios-h195-001b, Guangzhou Xinyuan Biotechnology Co., Ltd., Guangzhou, China). CAOV3 (#CAOV-3, Guangzhou Xinyuan Biotechnology Co., Ltd., Guangzhou, China), A2780 (#A2780, Guangzhou Xinyuan Biotechnology Co., Ltd., Guangzhou, China), and OVCAR8 (#OVCAR-8, Guangzhou Xinyuan Biotechnology Co., Ltd., Guangzhou, China) cells were maintained in Dulbecco's Modified Eagle Medium (DMEM) (#XY-9845, Guangzhou Xinyuan Biotechnology Co., Ltd., Guangzhou, China), Roswell Park Memorial Institute 1640 medium (RPMI-1640) (#XY-9846, Guangzhou Xinyuan Biotechnology Co., Ltd., Guangzhou, China), and RPMI-1640 medium, respectively. All media were supplemented with 10% fetal bovine serum (FBS) (#UBS283-04, Guangzhou Xinyuan Biotechnology Co., Ltd., Guangzhou, China) and 1% penicillin / streptomycin (P/S) (#15140122, Gibco, Grand Island, NY, USA). The cells were incubated at 37 ℃ in a humidified environment containing 5% CO_2. Once cells reached 80%–90% confluence, they were subcultured after digestion with 0.25% trypsin (#25200072, Gibco,

Grand Island, NY, USA). SKOV3, CAOV3, A2780, and OVCAR8 cell lines were authenticated by short tandem repeat profiling and were routinely confirmed to be free of mycoplasma contamination using the MycoSEQ™ Mycoplasma Detection Kit (#4460623, Thermo Fisher Scientific, Waltham, MA, USA).

Generation of Niraparib-Resistant SKOV3 Cell Line

The SKOV3 cells were exposed to long-term induction through continuous cultivation in complete McCoy's 5A medium supplemented with 21 μM niraparib (#S2741, Selleck Chemicals, Houston, TX, USA), 10% FBS, and 1% P/S. During the six-month induction period, the niraparib-containing complete medium was renewed every three days to maintain consistent drug pressure. Cells were passaged at 80–90% confluence. By regularly observing the cell state and conducting continuous subculturing under constant drug pressure, a stable niraparib-resistant subline capable of continuous propagation was successfully developed.

Transcriptome Sequencing and Analysis

Parental SKOV3 cells (SKOV3_parent) and cells obtained after 2, 3, and 6 months of niraparib treatment (designated SKOV3_Nira_2M, SKOV3_Nira_3M, and SKOV3_Nira_6M, respectively) were collected, with three biological replicates per group. Total RNA was extracted using TRIzol reagent (#15596026CN, Thermo Fisher Scientific, Waltham, MA, USA) and treated with DNase I (#M0303S, New England Biolabs, Ipswich, MA, USA) to remove genomic DNA contamination. RNA concentration and purity were measured using a NanoDrop 2000 spectrophotometer (Thermo Fisher Scientific, Wilmington, DE, USA), and integrity was assessed with an Agilent 2100 Bioanalyzer (Agilent Technologies, Santa Clara, CA, USA), ensuring an RNA Integrity Number (RIN) >7.0. Sequencing libraries were constructed using the NEBNext® Ultra™ II RNA Library Prep Kit for Illumina® (#E7770S, New England Biolabs, Ipswich, MA, USA). Qualified libraries were subjected to PE150 sequencing on an Illumina NovaSeq 6000 platform (Illumina, San Diego, CA, USA). Raw sequencing data were processed for quality control using fastp (v0.23.2; BGI, Shenzhen, China) to obtain high-quality clean reads. Clean reads were aligned to the human reference genome GRCh38/hg38 using HISAT2 (v2.2.1; Johns Hopkins University, Baltimore, MD, USA), followed by transcript assembly and expression quantification (in Transcripts Per Million, TPM) using StringTie (v2.2.1; Johns Hopkins University, Baltimore, MD, USA). Differential expression genes (DEG) analysis was performed using the "limma" package (v3.52.4; Bioconductor, maintained by Fred Hutchinson Cancer Research Center, Seattle, WA, USA) in R (v4.2.0; R Foundation for Statistical Computing, Vienna, Austria), with a screening threshold of $|\log_2$ fold change$| > 1$ and $p < 0.05$. Heatmaps of DEG were generated using the "pheatmap" package (v1.0.12; CRAN, maintained by R Foundation for Statistical Computing, Vienna, Austria). Gene sets related to DNA damage repair and other relevant pathways were retrieved from the Molecular Signatures Database (MSigDB) to create faceted heatmaps. Overlaps of DEG across different resistance stages were analyzed and visualized using the "VennDiagram" package (v1.7.3; CRAN, maintained by R Foundation for Statistical Computing, Vienna, Austria). Based on The Cancer Genome Atlas (TCGA)-OC data, Kaplan-Meier survival analysis for key genes was conducted using the "survival" (v3.4-0; originally by Terry Therneau, Mayo Clinic, Rochester, MN, USA) and "survminer" (v0.4.9; CRAN, maintained by R Foundation for Statistical Computing, Vienna, Austria) packages.

SiRNA Synthesis and Cell Transfection

SiRNA sequences targeting *PARP1* (siNC: 5′-UUCUCCGAACGUGUCACGUTT-3′ (sense), 5′-ACGUGACACGUUCGGAGAATT-3′ (antisense); siPARP1-1: 5′-ACUUUUCCAUCAAACAUGGGC-3′ (sense), 5′-CCAUGUUUGAUGGAAAAGUCC-3′ (antisense); siPARP1-2: 5′-AUUUCUCGGAAUUCCUUUGGG-3′ (sense), 5′-CAAAGGAAUUCCGAGAAAUCUU-3′ (antisense)) were chemically synthesized by Sangon Biotech (Shanghai, China). Exponentially growing SKOV3 cells were seeded into appropriate culture plates and transfected when they reached 60–70% confluence. According to the manufacturer's protocol, the siRNAs and Lipofectamine 3000 transfection reagent (#L3000150, Thermo Fisher Scientific, Waltham, MA, USA) were separately diluted in serum-free medium, incubated at 25 ℃ for 5 minutes, and then combined to form transfection complexes. The complexes were further incubated at 25 ℃ for an additional 20 minutes and subsequently added dropwise and evenly distributed to the cell culture wells, which had been replenished with serum-free or low-serum medium. After 6 hours of transfection, the medium was replaced with complete medium with or without niraparib for continued culture. At 72 hours post-transfection, cells were harvested, and the gene knockdown efficiency was validated via quantitative reverse transcription polymerase chain reaction (qRT-PCR) or Western blot analysis.

Construction and Validation of the PARP1 Overexpression Vector

Primers containing XhoI and PmeI restriction sites were designed based on the human *PARP1* coding sequence (NM_001618.4) and synthesized by Sangon Biotech (Shanghai, China). The *PARP1* fragment was amplified by PCR using SKOV3 cell cDNA as the template and PrimeSTAR HS DNA polymerase (#R044Q, Takara Bio, Otsu, Shiga, Japan). In parallel, the pcDNA3.1-HA empty vector (#128034; http://n2t.net/addgene:128034; RRID: Ad-

dgene_128034; Addgene, Watertown, MA, USA) was linearized by double digestion with XhoI (#R0146S, New England Biolabs, Ipswich, MA, USA) and PmeI (#R0560S, New England Biolabs, Ipswich, MA, USA) restriction enzymes, and the linearized fragment was purified. The purified insert and vector were mixed at a 3:1 molar ratio and ligated using T4 DNA ligase (#EL0014, Thermo Fisher Scientific, Waltham, MA, USA) at 16 °C overnight. The ligation product was transformed into DH5α competent cells (#C2987H, New England Biolabs, Ipswich, MA, USA), and transformants were screened on LB agar plates containing ampicillin (#L2010, Solarbio, Beijing, China). Single colonies were subjected to initial screening by colony PCR, followed by plasmid extraction (#DP103, Tiangen Biotech, Beijing, China). Positive clones were verified by XhoI/PmeI double digestion and subsequently sent to Sangon Biotech for Sanger sequencing. The confirmed recombinant plasmid, pcDNA3.1-HA-*PARP1*, was transfected into SKOV3 cells using Lipofectamine 3000 for subsequent experiments.

Niraparib Sensitivity Assay

Exponentially growing SKOV3_parent, SKOV3_Nira_6M, CAOV3, A2780, and OVCAR8 cells were trypsinized, harvested, and resuspended. Cells were then seeded into 96-well plates (#351172, Corning, Corning, NY, USA) at a density of 1×10^4 cells per well in 100 µL of complete medium. The plates were incubated for 24 hours to allow for cell attachment. Subsequently, SKOV3_parent, SKOV3_Nira_6M, and OVCAR8 cells were treated by replacing the medium with fresh complete medium containing either dimethyl sulfoxide (DMSO) (#D8418, Sigma-Aldrich, St. Louis, MO, USA) (vehicle control) or niraparib at specified concentrations (1, 10, 100, 500, and 1000 µM). Specifically, A2780 cells were exposed to 0.47, 0.94, 1.875, 3.75, 7.5, 15, 30, 60, and 120 µM niraparib, while CAOV3 cells were treated with 0, 12.5, 18.75, 25, 37.5, 50, 75, 100, 150, 200, and 300 µM niraparib. After 72 hours of drug treatment, 10 µL of cell counting kit-8 (CCK-8) reagent (#C0037, Beyotime, Shanghai, China) was added to each well under light-protected conditions, followed by incubation at 37 °C for 4 hours. The absorbance of each well was then measured at a wavelength of 450 nm using a Varioskan™ Flash multifunctional microplate reader (Thermo Fisher Scientific, Waltham, MA, USA). The mean optical density (OD) and standard deviation for each group were calculated from the raw data. Dose-response curves were plotted, and the half-maximal inhibitory concentration (IC_{50}) was calculated.

Crystal Violet Staining for Cell Viability Assay

Exponentially growing SKOV3 cells (1×10^4 cells/mL, 100 µL/each well) subjected to different treatments were seeded into a 96-well cell culture plate and pre-cultured for 24 hours. Among these, SKOV3_parent cells were then divided into eight groups, including control (CON) group (no drug treatment), Niraparib group (treated with 21 µM niraparib for 72 hours), siNC group (transfected with siRNA NC sequence), siNC+Niraparib group, siPARP1 groups (transfected with *PARP1* siRNA-1 or siRNA-2 sequences), and siPARP1s+Niraparib groups (co-treated with *PARP1* siRNA-1 or siRNA-2 transfection and 21 µM niraparib). SKOV3 cells subjected to long-term niraparib treatment were divided into four groups, including ovNC group (transfected with empty plasmid vector), ovNC+Niraparib group (treated with 80 µM niraparib and empty plasmid vector), ovPARP1 group (transfected with *PARP1* overexpression plasmid vector), and ovPARP1+Niraparib group (co-treated with *PARP1* overexpression plasmid transfection and 80 µM niraparib). In addition, to compare the proliferative capacity of cells at different stages of niraparib resistance, SKOV3_parent, SKOV3_Nira_2M, SKOV3_Nira_3M, and SKOV3_Nira_6M cells were treated with 1, 10, or 100 µM niraparib alone. After 72 hours of treatment, cells in each well were fixed with 100 µL of pre-cooled 4% paraformaldehyde (#P6148, Sigma-Aldrich, St. Louis, MO, USA) for 15 minutes. Subsequently, cells were stained with 100 µL of 0.5% crystal violet staining solution (#61135, Sigma-Aldrich, St. Louis, MO, USA) for 20 minutes. Cell status was observed, and crystal violet staining images were acquired under a microscope (Olympus, Tokyo, Japan). Thereafter, 100 µL of 33% glacial acetic acid (#1005706, Sigma-Aldrich, St. Louis, MO, USA) was added to each well to dissolve the dye, followed by shaking for 15 minutes. Absorbance was measured at a wavelength of 570 nm using a multifunctional microplate reader. After subtracting the average OD value of blank control wells, the relative cell viability (%) was calculated. Each group was set up with 4 replicate wells.

EdU Staining for Cell Proliferation

SKOV3_parent and niraparib-resistant cell lines were treated with *PARP1* siRNAs or overexpression vectors in combination with niraparib for 72 hours, followed by incubation with 100 µL per well of EdU working solution (#C10339, Click-iT EdU Kit, Thermo Fisher Scientific, Waltham, MA, USA) for 2 hours. Cells were then fixed with 4% paraformaldehyde, permeabilized with glycine (#62011516, Sinopharm Chemical Reagent Co., Ltd., Shanghai, China) and PBS containing 0.5% Triton X-100 (#X100, Sigma-Aldrich, St. Louis, MO, USA) for 20 minutes. According to the kit instructions, 50 µL Click reaction mixture and 100 µL DAPI nuclear staining solution (#D9542, Sigma-Aldrich, St. Louis, MO, USA) were sequentially added and incubated in the dark for 30 and 15 minutes, respectively. Images were acquired using a fluorescence microscope (Olympus, Tokyo, Japan), with five random fields captured per well. The percentage of EdU-

positive cells was calculated using ImageJ software (National Institutes of Health, Bethesda, MD, USA).

Apoptosis Detection by Flow Cytometry (Annexin V-FITC/PI Double Staining)

SKOV3_parent and niraparib-resistant cells subjected to various treatments were collected and resuspended to a density of 1–2 × 10^6 cells/mL. A 100 µL aliquot of the cell suspension was sequentially stained with 5 µL of Annexin V-FITC and 5 µL of propidium iodide (PI) staining solution (from the Annexin V-FITC/PI Apoptosis Detection Kit; #E606336, Sangon Biotech, Shanghai, China), followed by incubation in the dark for 15 and 5 minutes, respectively. After staining, 500 µL of pre-chilled binding buffer was immediately added to each sample. Analysis was performed using a flow cytometer (BIO-RAD, Hercules, CA, USA) with an excitation wavelength of 488 nm. Unstained and single-stained cell samples were used as controls for compensation and gating. Data were analyzed with FlowJo software (FlowJo LLC, Ashland, OR, USA), and the total apoptosis rate (%) was calculated.

Western Blot Analysis of PARP1 Protein Expression

To assess PARP1 protein levels, SKOV3_parent and SKOV3_Nira_6M cells were harvested and lysed using RIPA buffer (#20-188, Millipore, Billerica, MA, USA) supplemented with protease inhibitors (#04693124001, Roche, Basel, Switzerland). Total protein concentration was determined using a BCA Protein Assay Kit (#KTD3001, Abbkine, Wuhan, China). Equal amounts of protein (20 µg) were separated by electrophoresis on 10% SDS-PAGE gels (#G2037-50T, Servicebio, Wuhan, China) and subsequently transferred onto a nitrocellulose membrane (#FFN56, Betoyime, Shanghai, China) using a semi-dry transfer system (BIO-RAD, Hercules, CA, USA). The membrane was blocked with 5% bovine serum albumin (#A1933-25G, Sigma-Aldrich, St. Louis, MO, USA) for 1 hour at 25 ℃. Immunoblotting was performed by incubating the membrane overnight at 4 °C with a rabbit anti-PARP1 primary antibody (1:1000; #9542, Cell Signaling Technology, Danvers, MA, USA). After washing, the membrane was incubated with a horseradish peroxidase-conjugated goat anti-rabbit secondary antibody (1:1000; #ab6721, Abcam, Cambridge, UK) for 1 hour at 25 ℃. Protein bands were visualized using an enhanced chemiluminescence (ECL) substrate (#WBULS0500, Millipore, Billerica, MA, USA) and imaged with a chemiluminescence detection system (Bio-Rad ChemiDoc, Hercules, CA, USA). GAPDH (anti-GAPDH antibody, 1:1000; #2118, Cell Signaling Technology) was used as a loading control for normalization, and band intensity was quantified by densitometric analysis.

Immunofluorescence Staining

SKOV3 cells were seeded onto sterile glass coverslips in 24-well plates and cultured until approximately 70% confluence. After gentle washing with ice-cold PBS, cells were fixed with 4% paraformaldehyde for 15 minutes. Permeabilization was carried out using PBS containing 0.3% Triton X-100 for 15 minutes. Non-specific binding sites were blocked with 5% bovine serum albumin (BSA) in PBS for 1 hour at RT. Cells were then incubated overnight at 4 ℃ in a humidified chamber with rabbit anti-PARP1 primary antibody (1:200; #ab227244, Abcam, Cambridge, UK). Following extensive washing with PBS, cells were incubated with Alexa Fluor 594-conjugated goat anti-rabbit IgG (1:500; #111-585-144, AmyJet Scientific Inc., Wuhan, China) for 1 hour at RT in the dark. Nuclei were counterstained with DAPI (300 nM) for 5 minutes. Finally, the coverslips were mounted onto glass slides using an antifade mounting medium. All images were captured under identical imaging parameters using a laser scanning confocal fluorescence microscope.

Real-Time Quantitative PCR Analysis of Gene Expression

Total RNA was extracted from treated cells using TRIzol reagent. The RNA concentration and purity were determined using a NanoDrop 2000 spectrophotometer. Subsequently, 1 µg of total RNA was reverse transcribed into cDNA using the PrimeScript™ RT Master Mix kit (#RR036A, Takara Bio, Otsu, Shiga, Japan). Real-time quantitative PCR was performed on a QuantStudio 5 real-time PCR system (Applied Biosystems, Thermo Fisher Scientific, Waltham, MA, USA) using TB Green Premix Ex Taq II (#RR820A, Takara Bio, Otsu, Shiga, Japan) and gene-specific primers for *PARP1* (F: 5′-CGGAGTCTTCGGATAAGCTCT-3′, R: 5′-TTTCCATCAAACATGGGCGAC-3′), *PARP2* (F: 5′-TGCCCAGAGGAACTTCAGTG-3′, R: 5′-TTGGTGGCATAGTCCATCTGT-3′) and *PARP3* (F: 5′-GACCAACATCGAGAACAACAACA-3′, R: 5′-GCCTTGTGAAGTGGTTGATCT-3′). The thermal cycling conditions were as follows: initial denaturation at 95 °C for 30 seconds, followed by 40 cycles of 95 °C for 5 seconds and 60 °C for 30 seconds. Each sample was assayed in triplicate. The relative expression of the target gene was calculated using the $2^{-\Delta\Delta Ct}$ method, with *GAPDH* (F: 5′-GGAGCGAGATCCCTCCAAAAT-3′, R: 5′-GGCTGTTGTCATACTTCTCATGG-3′) serving as the internal reference for normalization.

Construction of Doxycycline-Inducible Stable Cell Lines

To validate the function of *PARP1 in vivo*, a doxycycline (DOX)-inducible gene regulation system was established. First, shRNA oligonucleotides targeting the validated siPARP1-2 sequence were synthesized (Sangon Biotech, Shanghai, China) and cloned into the lentiviral

inducible vector pLVX-TetOne-Puro (#631847, Clontech, San Jose, CA, USA), which contains a TRE3G promoter, to construct the DOX-inducible *PARP1* knockdown vector (pLVX-TetOne-sh*PARP1*). Concurrently, the full-length coding sequence of human *PARP1* was cloned into another inducible vector, pLVX-TRE3G (#631363, Clontech, San Jose, CA, USA), to generate the DOX-inducible *PARP1* overexpression vector (pLVX-TRE3G-*PARP1*). Lentiviral particles were then packaged using a three-plasmid system (transfer plasmid, packaging plasmid psPAX2, and envelope plasmid pMD2.G, all from Addgene, Watertown, MA, USA) in HEK293T cells (#293T, Guangzhou Xinyuan Biotechnology Co., Ltd., Guangzhou, China) via polyethylenimine (#24765, Polysciences, Warrington, PA, USA) transfection. The viral supernatant was collected, concentrated by ultracentrifugation, and titrated. The concentrated viruses were used to infect SKOV3_Nira_6M resistant cells and their parental cells. Following infection, stable cell lines were selected using puromycin (#P4512, Sigma-Aldrich, St. Louis, MO, USA). Finally, the efficiency of DOX-induced PARP1 knockdown or overexpression was confirmed by treating the stable cells with DOX (Sigma-Aldrich, St. Louis, MO, USA) and analyzing protein levels via Western blotting.

Establishment of Subcutaneous Xenograft Tumor Models in Mice

Stable cell lines with DOX-inducible gene expression (5×10^6 cells) were subcutaneously inoculated into the right flank of 4–6-week-old female BALB/c nude mice (Beijing Vital River Laboratory Animal Technology Co., Ltd., Beijing, China). Starting from the first day post-inoculation, DOX was administered to the experimental groups via drinking water containing 2 mg/mL DOX to induce PARP1 expression changes *in vivo*. Selected groups also received niraparib treatment via oral gavage. Approximately 7 days after inoculation, tumor growth was monitored by measuring the tumor length (L) and width (W) twice a week using a digital caliper. Tumor volume was calculated using the formula: $V = (L \times W^2) / 2$. Mouse body weight was also recorded during the monitoring period. This study was conducted in accordance with the ARRIVE guidelines 2.0. BALB/c nude mice were housed under specific pathogen-free conditions. Animals were randomly assigned to experimental groups (n = 6 per group) using a random number table. Tumor measurements and endpoint assessments were performed by investigators blinded to group allocation. The humane endpoints were defined as follows: tumor volume exceeding 1500 mm^3, severe ulceration or necrosis, body weight loss >20%, or signs of severe distress. Mice reaching endpoint criteria were euthanized by CO_2 inhalation followed by cervical dislocation. All animal experiments were conducted in a specific pathogen-free barrier facility and performed in accordance with relevant animal care and use guidelines.

Molecular Docking Study

The crystal structures of the catalytic domains of human PARP1 (PDB: 7KK5), PARP2 (PDB: 7AEO), and PARP3 (PDB: 4GV0) were retrieved from the RCSB PDB database. The three-dimensional structure of niraparib was obtained from the PubChem database (CID: 135565138). Protein receptors were prepared using the PyMOL molecular graphics system (Schrödinger, Inc., New York, USA) by removing water molecules and original ligands. Both the protein receptors and the niraparib ligand were preprocessed using AutoDock Tools 1.5.7 (The Scripps Research Institute, La Jolla, CA, USA), which included adding hydrogen atoms and assigning charges. Semi-flexible docking calculations were conducted using AutoDock Vina (v1.2.0, The Scripps Research Institute, La Jolla, CA, USA), with the protein held rigid and the small molecule ligand allowed conformational flexibility. The conformation with the lowest predicted binding free energy was selected for subsequent analysis. Finally, the optimal binding conformation was visualized in PyMOL, and the interactions between niraparib and the protein active site residues were analyzed and quantified.

Statistical Analysis

All experiments were independently performed in triplicate. Data were analyzed using GraphPad Prism version 10.0 (GraphPad Software, San Diego, CA, USA). Normality was first assessed using the Shapiro-Wilk test. For data that followed a normal distribution and exhibited homogeneity of variances (assessed by F-test), pairwise comparisons were performed using the unpaired *t*-test. In cases of heteroscedasticity, Welch's *t*-test was applied. For data that did not meet the assumption of normality, the Mann-Whitney U test was used. A *p*-value of less than 0.05 was considered statistically significant.

Results

Long-Term Niraparib Treatment Induces Acquired Resistance in BRCA1/2-Wild Type Ovarian Cancer Cells

To explore the mechanisms of acquired resistance to niraparib in BRCAwt ovarian cancer, this study first established a niraparib-resistant SKOV3 cell line through long-term drug pressure induction. Unlike the commonly used stepwise dose-escalation method [17,18], a constant, relatively high concentration (21 μM) of niraparib was applied continuously for 6 months (Fig. 1A), yielding a stable resistant cell line (SKOV3_Nira_6M) with a resistance index of 5.35 (IC_{50}: 86.51 μM vs. 16.16 μM for parental cells) (Fig. 1B). Crystal violet staining and EdU proliferation assays further demonstrated that, compared to the parental cells and the cells treated with niraparib for 2 months (SKOV3_Nira_2M) and 3 months (SKOV3_Nira_3M), SKOV3_Nira_6M exhibited signifi-

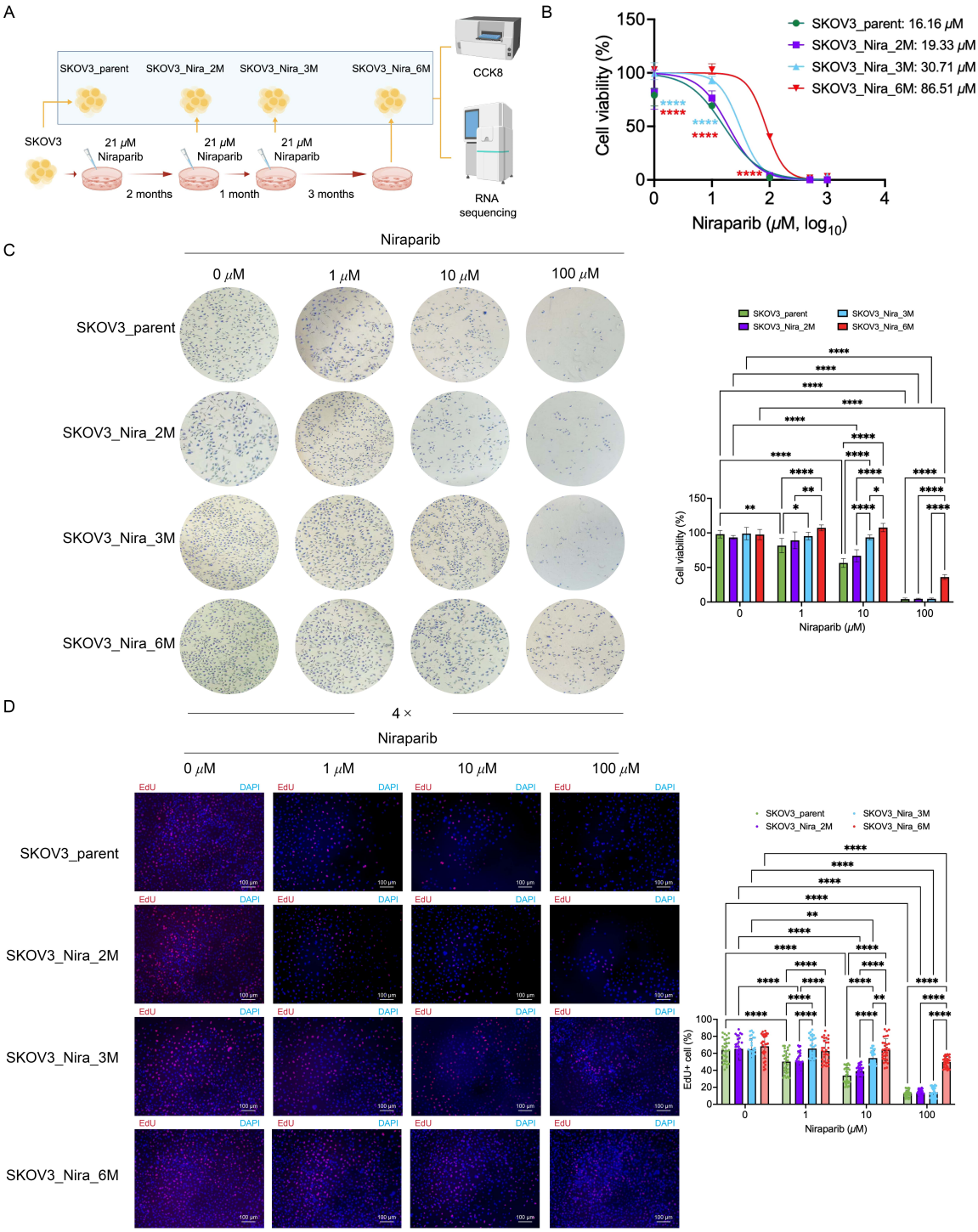

Fig. 1. Induction of acquired resistance to niraparib in ovarian cancer cells following long-term treatment. (A) Schematic illustration of the generation of niraparib-resistant cell lines. (B) Dose-response curves of parental cells and cells treated with niraparib for 2, 3, and 6 months, as determined by CCK-8 assay (n = 3 independent experiments, with 5 replicates per experiment). (C) Quantitative analysis of relative cell viability assessed using crystal violet staining after treatment with the indicated concentrations of niraparib (0, 1, 10, 100 μM) for 72 hours (n = 3 independent experiments, with 3 replicates per experiment). (D) Quantitative analysis of cell proliferation rate determined by EdU staining after 72-hour treatment with the indicated concentrations of niraparib (n = 3 independent experiments). Data are presented as mean ± standard deviation. * $p < 0.05$; ** $p < 0.01$; **** $p < 0.0001$. In figure B, blue **** denotes SKOV3_parent *vs.* SKOV3_Nira_3M; red **** denotes SKOV3_parent *vs.* SKOV3_Nira_6M ($p < 0.0001$). CCK-8, cell counting kit-8; EdU, 5-ethynyl-2′-deoxyuridine.

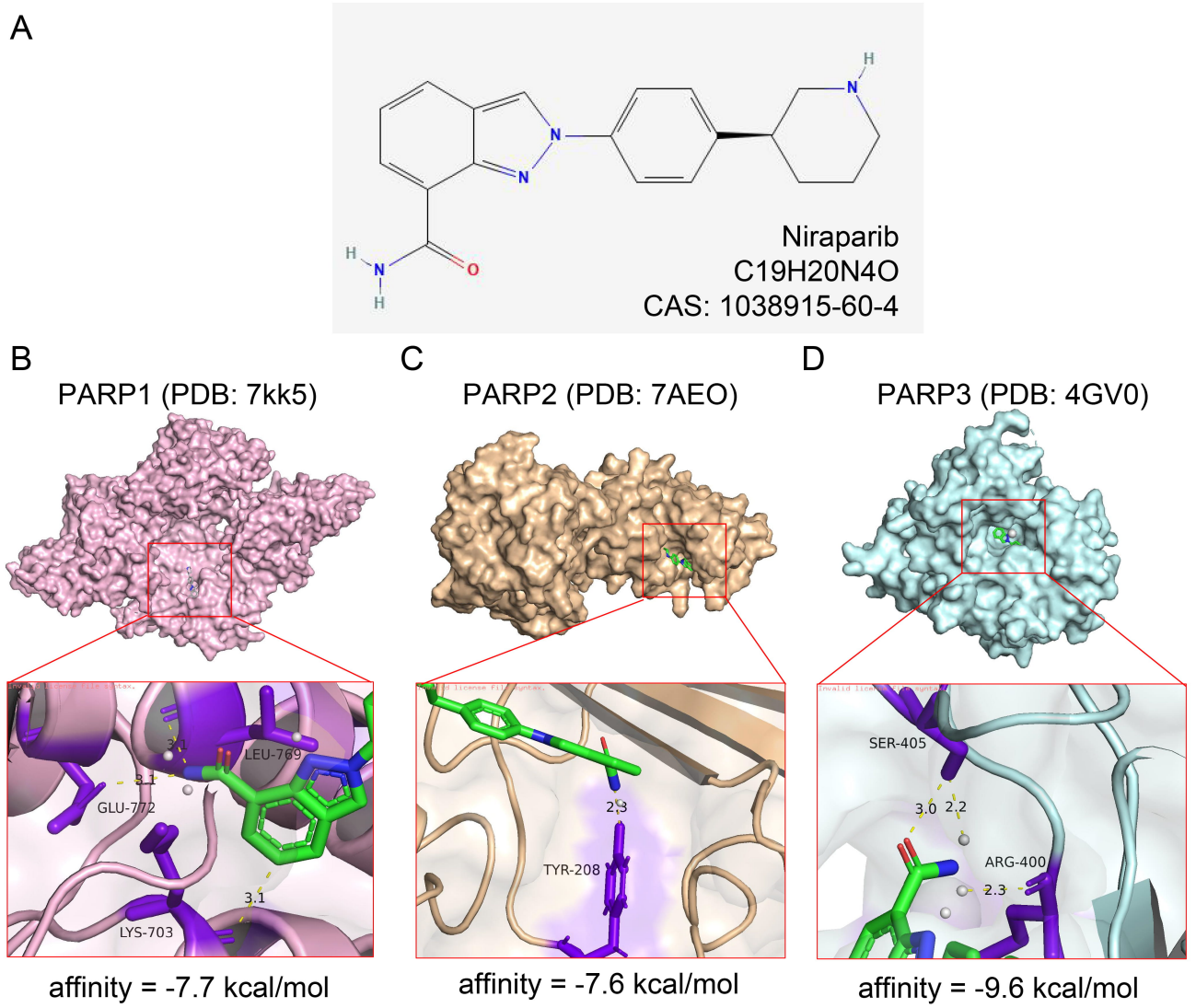

Fig. 2. Analysis of the binding modes of Niraparib to PARP1, PARP2, and PARP3. (A) Chemical structure of Niraparib. (B–D) Schematic representation of the complex structures and key interactions between Niraparib and PARP1 (PDB: 7KK5) (B), PARP2 (PDB: 7AEO) (C), PARP3 (PDB: 4GV0) (D) based on molecular docking simulations. PARP, Poly(ADP-ribose) polymerase; PDB, Protein Data Bank.

cantly enhanced survival ($p < 0.05$, Fig. 1C) and proliferative capacity ($p < 0.01$, Fig. 1D) under treatment with 1, 10, and 100 μM niraparib, confirming its resistant phenotype.

Binding Characteristics of Niraparib to PARP Family Proteins and Their Expression Changes in Resistant Cells

PARP1, PARP2, and PARP3 are core enzymes that mediate Poly(ADP-ribosyl)ation (PARylation) and play critical roles in DNA damage repair pathways [19]. Niraparib, as a highly selective PARP1/2 inhibitor, demonstrates high-affinity binding to the catalytic domains of its target proteins in molecular docking simulations. Specifically, the calculated binding free energies of niraparib to PARP1 (PDB: 7KK5) and PARP2 (PDB: 7AEO) were –7.7 kcal/mol (Fig. 2A,B) and –7.6 kcal/mol (Fig. 2C), respectively, indicating comparable binding strengths. Within PARP1, niraparib penetrates deep into the active site pocket, interacting with key residues such as GLU772, LEU769, and LYS703, a binding mode consistent with previously reported crystal structures [20]. In PARP2, niraparib forms a strong interaction (2.3 Å) with the catalytic triad residue TYR208 (Fig. 2C), directly competing for and occupying the NAD^+ substrate binding site, which structurally explains its potent enzyme inhibitory mechanism.

Although docking predicted an even lower binding free energy for niraparib with PARP3 (PDB: 4GV0) at –9.6 kcal/mol, along with tight hydrophilic interactions with SER405 and ARG400 (Fig. 2D), its biochemical inhibitory activity ($IC_{50} \approx 1.3$ μM) is significantly weaker than its nanomolar-level inhibition of PARP1/2 (IC_{50} values of 2.1 nM and 3.8 nM, respectively) [21,22]. This discrepancy

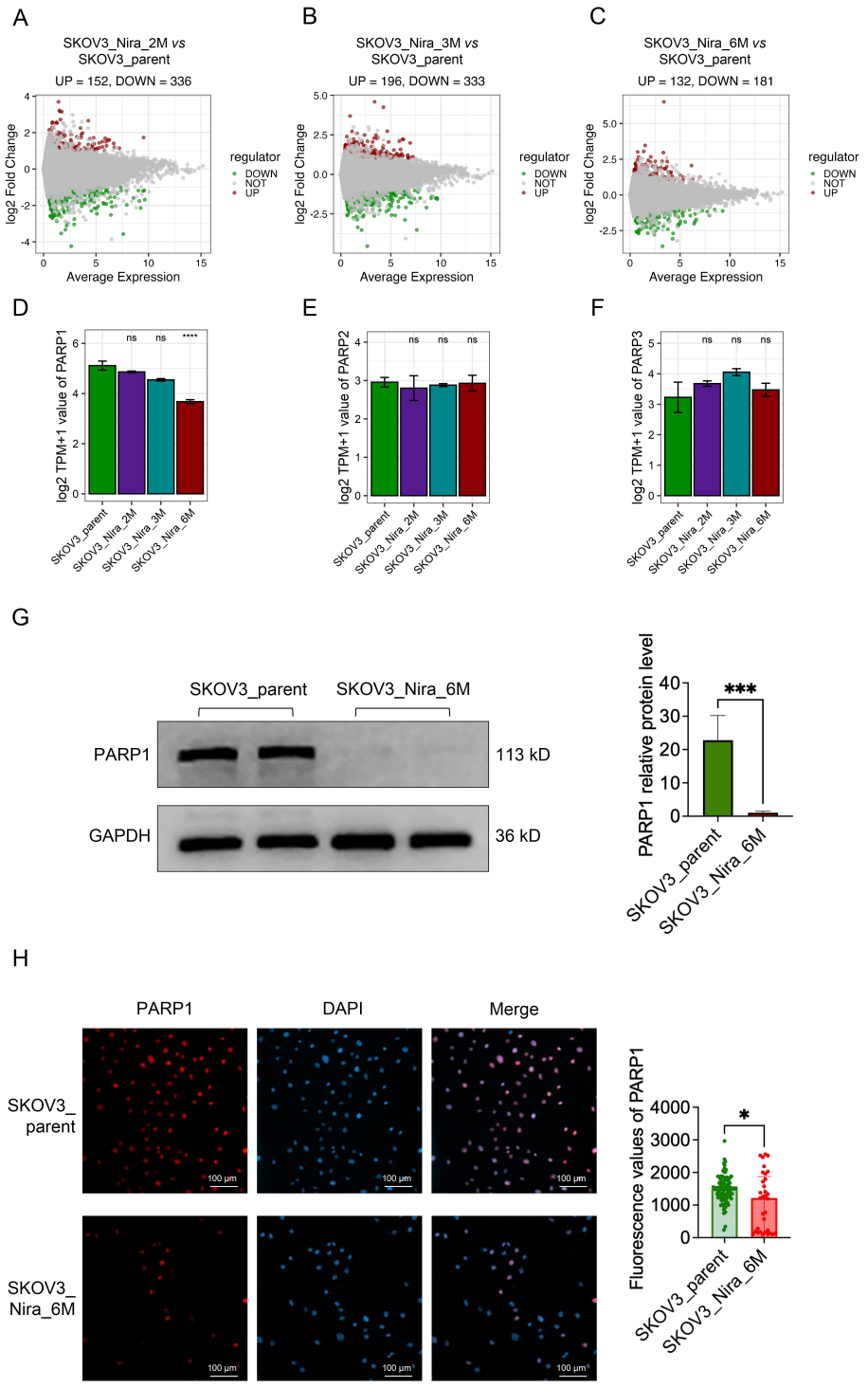

Fig. 3. Expression alterations of the PARP inhibitor target *PARP1* in niraparib-resistant ovarian cancer cells. (A–C) Volcano plots showing differentially expressed genes in the transcriptome of SKOV3 cells after long-term treatment with niraparib for 2 (A), 3 (B), and 6 (C) months, compared to parental cells (n = 3 per group). (D–F) Relative mRNA expression levels of *PARP1* (D), *PARP2* (E), and *PARP3* (F) in SKOV3 cells treated with niraparib for the indicated durations (2, 3, 6 months) (n = 3 per group). (G,H) Western blotting (G) and immunofluorescence (H) analysis of PARP1 protein levels in SKOV3 cells treated with niraparib for different periods (n = 3 independent experiments, with 4 replicates per experiment). Quantitative data from Western blotting are presented as mean ± standard deviation, while fluorescence-based quantitative data are shown as median (25th–75th percentiles). ns $p > 0.05$; * $p < 0.05$; *** $p < 0.001$; **** $p < 0.0001$.

may be related to the absence of the key D-loop domain in PARP3 [19], which is present in PARP1/2 and is crucial for stabilizing the inhibitor-bound conformation and achieving efficient enzyme inhibition. This suggests that static docking scores cannot fully reflect the dynamic inhibitory efficacy of enzymes.

As the direct targets of niraparib, changes in PARP protein expression may be linked to "target escape" mechanisms underlying acquired resistance. Our transcriptomic and protein-level analyses (Fig. 3A–H) revealed that under prolonged niraparib pressure, only *PARP1* exhibited a specific and significant downregulation at both the mRNA ($p < 0.0001$; Fig. 3D) and protein ($p < 0.05$; Fig. 3G,H) levels in the highly resistant SKOV3_Nira_6M cells, with no significant changes observed in the early resistance stages (2 and 3 months) or in parental cells ($p > 0.05$; Fig. 3D). In contrast, the transcriptional expression levels of *PARP2* and *PARP3* remained stable across all stages ($p > 0.05$; Fig. 3E,F). These results suggest that the specific downregulation of *PARP1*, leading to a "reduction in target abundance", may be a key mechanism underlying the acquisition of niraparib resistance in BRCAwt ovarian cancer.

In addition, this study conducted transcriptomic analyses to assess changes in pathways associated with DNA damage response (**Supplementary Figs. 1,2**), drug efflux (**Supplementary Fig. 3**), and cell cycle checkpoints (**Supplementary Fig. 4**), which are important mechanisms underlying PARP inhibitor resistance. The results showed that, within the DNA damage repair pathways, although multiple genes exhibited significant differential expression during the early stages of resistance (SKOV3_Nira_2M/Nira_3M), most returned to baseline levels in the stably resistant cell line (**Supplementary Fig. 1A–K** and **Supplementary Fig. 2A–H**). Only the NHEJ pathway-associated histone gene H2BC8 remained significantly downregulated in SKOV3_Nira_6M cells ($p < 0.05$; **Supplementary Fig. 1I**). In the transmembrane transport pathway, 54 differentially expressed genes were identified ($p < 0.05$; **Supplementary Fig. 3A–M**). However, classical efflux pumps (e.g., ABCB1) showed no significant change ($p > 0.05$; **Supplementary Table 1**). Similarly, differentially expressed genes related to the cell cycle checkpoint pathway were primarily characterized by transient alterations during the early induction phase (**Supplementary Fig. 4A–S**). Further analysis revealed that *S100A10* ($p < 0.01$; **Supplementary Fig. 3E**), *THBS1* ($p < 0.05$; **Supplementary Fig. 3H**) (involved in transmembrane transport), and H2BC8 (associated with both NHEJ and cell cycle checkpoint pathways) were significantly downregulated in the stably resistant cells, while *SLC43A3* was significantly upregulated ($p < 0.0001$; **Supplementary Fig. 3M**). However, the expression levels of these genes showed no significant correlation with either overall survival or disease-free survival in ovarian cancer patients ($p > 0.05$, **Supplementary Fig. 5A–H**). Compared with *S100A10*, *THBS1*, *SLC43A3*, and H2BC8, which exhibited altered expression in resistant cells, PARP1 downregulation demonstrated stronger statistical significance (**Supplementary Table 2**), suggesting that it may play a more central and direct role in mediating the drug-resistant phenotype.

PARP1 Deficiency Confers Acquired Niraparib Resistance in BRCA1/2 Wild-Type Ovarian Cancer Cells

To investigate whether *PARP1* deficiency mechanistically drives acquired resistance to niraparib in BRCAwt ovarian cancer, *PARP1* expression was efficiently silenced in SKOV3_parent cells using two independent siRNAs ($p < 0.0001$; Fig. 4A,B). *PARP1* knockdown alone exerted no significant effect on basal cell viability or proliferation, consistent with its established role in DNA damage repair and its dispensability under unperturbed growth conditions. However, upon niraparib treatment, *PARP1* depletion profoundly attenuated cellular drug sensitivity, as reflected by a marked elevation in IC_{50} values from 21.97 μM to 321.8 μM and 356.0 μM, respectively ($p < 0.0001$; Fig. 4C). Subsequent phenotypic analyses further corroborated these findings, demonstrating that *PARP1* knockdown significantly enhanced cell survival and proliferative capacity relative to niraparib treatment alone ($p < 0.05$; Fig. 4D,E).

To validate this finding in a more physiologically relevant context, we established a DOX-inducible *PARP1* shRNA stable knockdown cell line ($p < 0.0001$, Fig. 4F) and employed it in a subcutaneous xenograft model in athymic nude mice. Consistent with the *in vitro* data, DOX-induced PARP1 knockdown attenuated the antitumor efficacy of niraparib *in vivo*, as evidenced by increased tumor wet weight and volume in the combination treatment group compared with the niraparib-alone group ($p < 0.05$; Fig. 4G–I). These results collectively demonstrate, both *in vitro* and *in vivo*, that *PARP1* expression is indispensable for the cytotoxic effect of niraparib in SKOV3 cells.

To assess the generalizability of this observation beyond the SKOV3 cell line, we performed parallel validation in three additional BRCAwt ovarian cancer cell lines, including A2780, CAOV3, and OVCAR8. As shown in Fig. 5A–F, successful *PARP1* knockdown in each cell line ($p < 0.05$; Fig. 5A,C,E) led to a marked decrease in sensitivity to niraparib. Specifically, the IC_{50} increased from approximately 9.2 μM to over 100 μM in A2780 cells (Fig. 5B), from approximately 20 μM to 93 μM in CAOV3 cells (Fig. 5D), and from approximately 29 μM to over 210 μM in OVCAR8 cells (Fig. 5F). These consistent findings across multiple cell backgrounds demonstrate that transcriptional suppression of *PARP1* expression induces high-level resistance to niraparib.

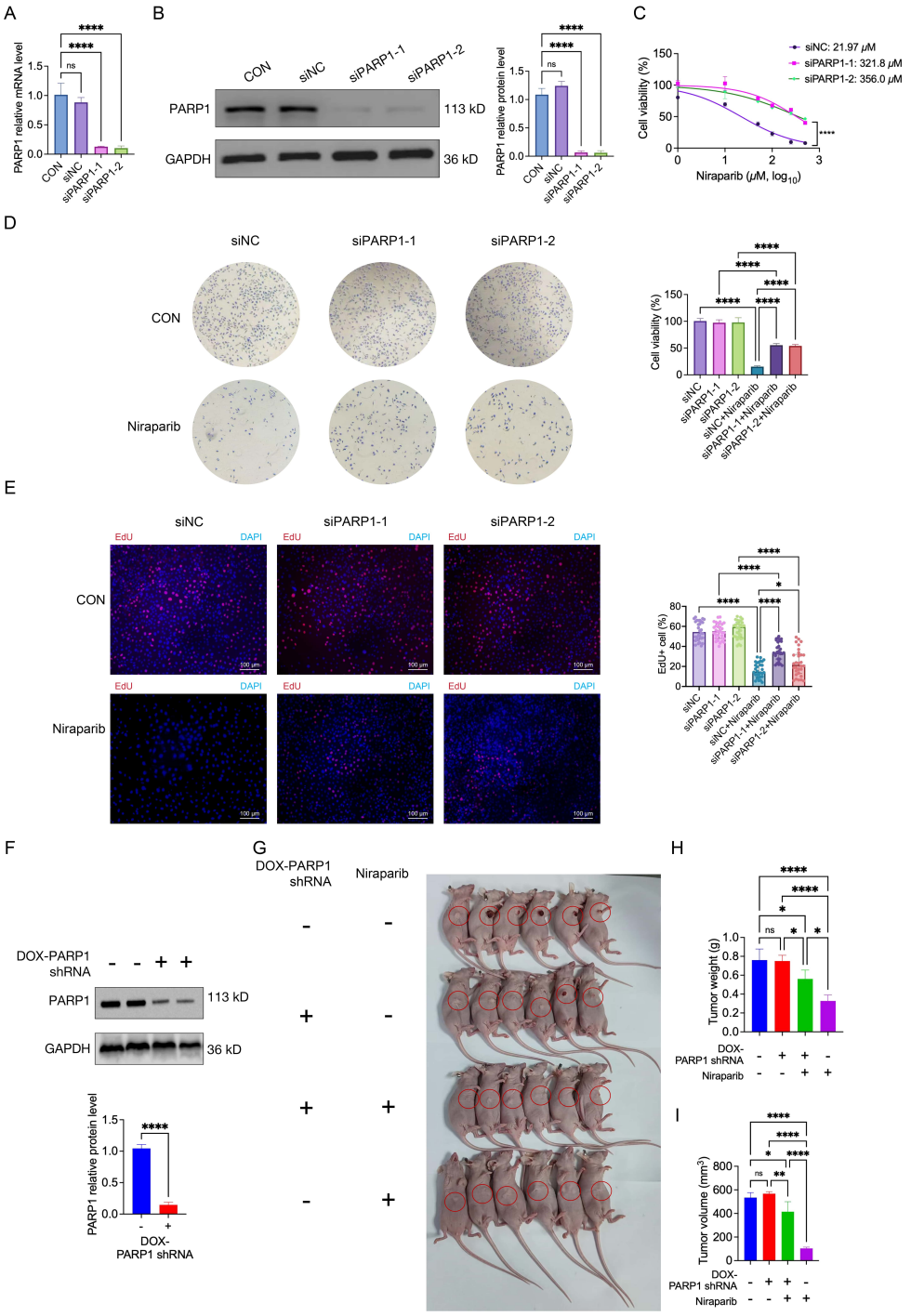

Fig. 4. Effect of *PARP1* interference on the inhibitory action of niraparib in ovarian cancer. (A,B) Changes in the relative mRNA (A) and protein (B) levels of *PARP1* 72 hours after transfection with siRNAs. (C) Dose-response curves of niraparib and cell viability in SKOV3_parent cells following *PARP1* knockdown by siRNAs. (D,E) Crystal violet staining images and quantitative analysis of cell viability (%) (D), and EdU staining images with quantitative analysis of cell proliferation rate (%) (E) in SKOV3_parent cells treated with *PARP1* siRNAs in combination with niraparib. (F) Interference efficiency of *PARP1* expression in SKOV3 cells after DOX-induced shRNA expression. (G–I) Subcutaneous tumor growth (G), tumor wet weight (H), and volume (mm^3, I) in nude mice after DOX-induced *PARP1* shRNA expression combined with niraparib treatment. All quantitative data are derived from three independent experiments, with 3–5 biological replicates per experiment. Results from EdU immunofluorescence staining are presented as the median (25th–75th percentiles), and all other data are expressed as mean ± standard deviation. ns $p > 0.05$; * $p < 0.05$; ** $p < 0.01$; **** $p < 0.0001$.

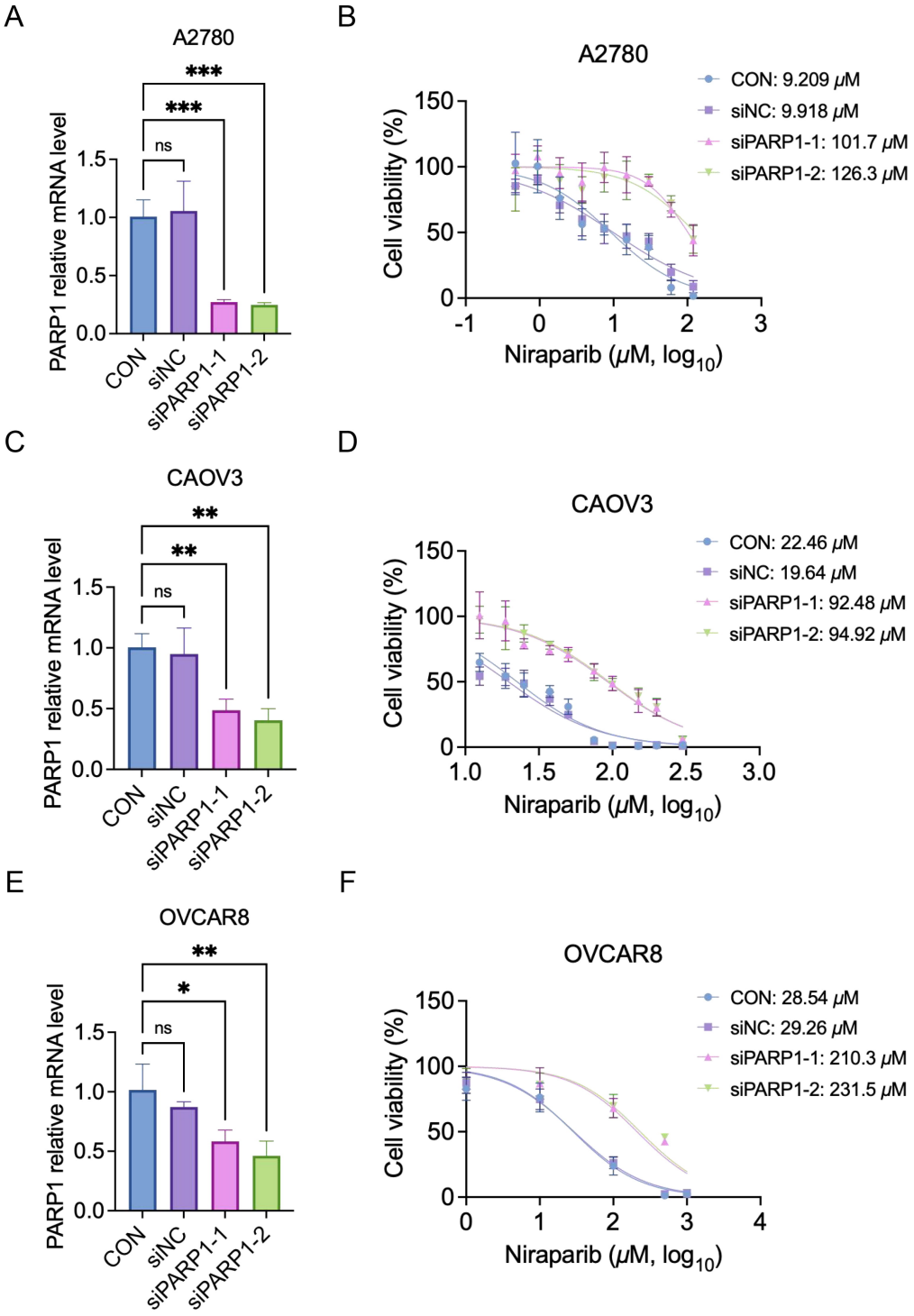

Fig. 5. Validation of *PARP1* low expression-induced reduction in niraparib sensitivity across multiple ovarian cancer cell lines. (A–F) Knockdown efficiency of *PARP1* by siRNA (A,C,E) and the corresponding niraparib dose-response curves (B,D,F) in A2780 (A,B), CAOV3 (C,D) and OVCAR8 (E,F). All quantitative data are derived from three independent experiments, with 3–5 biological replicates per experiment. All data are expressed as mean ± SD. ns $p > 0.05$; * $p < 0.05$; ** $p < 0.01$; *** $p < 0.001$.

Overexpression of PARP1 Partially Reverses Acquired Resistance to Niraparib in BRCA1/2 Wild-Type Ovarian Cancer

To further validate the pivotal role of *PARP1* in niraparib resistance within BRCAwt ovarian cancer, we examined whether restoration of *PARP1* expression was sufficient to reverse the drug-resistant phenotype. Experimental results demonstrated that forced expression of a *PARP1* overexpression construct resulted in robust upregulation of both mRNA and protein levels of *PARP1* in the resistant

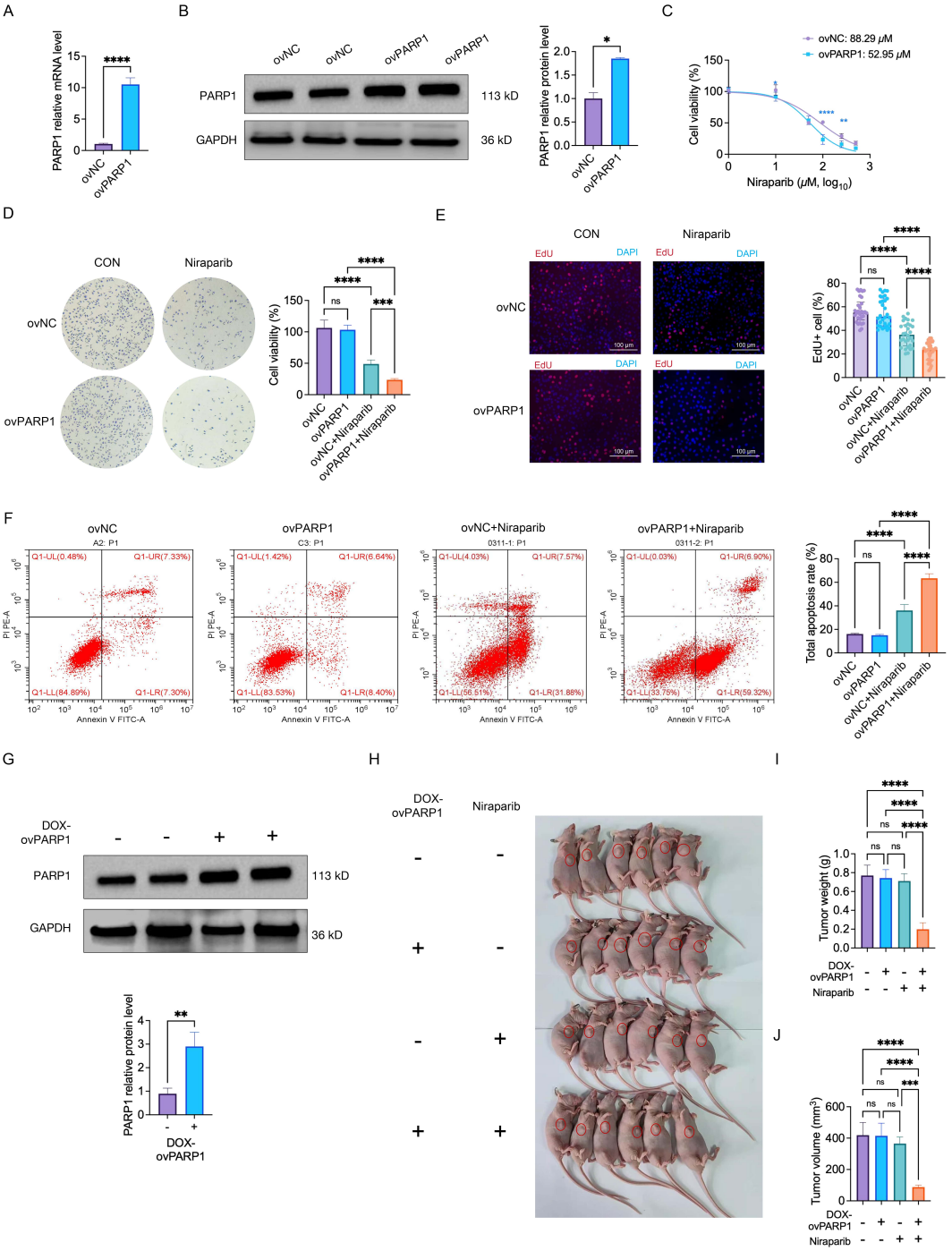

Fig. 6. Effect of *PARP1* overexpression on the inhibitory action of niraparib in resistant ovarian cancer. (A,B) Changes in the relative mRNA (A) and protein (B) levels of *PARP1* 72 hours after transfection with the overexpression vector. (C) Dose-response curves of niraparib and cell viability in parental SKOV3 cells following *PARP1* overexpression. (D–F) Crystal violet staining images and quantitative analysis of cell viability (%) (D), EdU staining images with quantitative analysis of cell proliferation rate (%) (E), and changes in total apoptosis rate (F) in parental SKOV3 cells treated with *PARP1* overexpression in combination with niraparib. (G) Overexpression efficiency of PARP1 in SKOV3 cells after DOX induction. (H–J) Subcutaneous tumor growth (H), tumor wet weight (I), and volume (mm^3, J) in nude mice after DOX-induced *PARP1* overexpression combined with niraparib treatment. All data points were obtained from three biologically independent experiments, each performed with 3–5 replicates. Values from EdU staining are reported as the median with interquartile range (25th–75th percentiles), whereas remaining quantitative results are shown as mean ± standard deviation. ns $p > 0.05$; * $p < 0.05$; ** $p < 0.01$; *** $p < 0.001$; **** $p < 0.0001$.

SKOV3_Nira_6M cells ($p < 0.05$; Fig. 6A,B). Functionally, overexpression of *PARP1* significantly resensitized cells to niraparib, reducing the IC_{50} value from 88.29 μM in the vector control group to 52.95 μM (Fig. 6C). Further phenotypic analysis confirmed that, compared to niraparib treatment alone, combining it with *PARP1* overexpression more effectively inhibited cell viability and proliferation and elicited a significantly elevated apoptotic rate ($p < 0.001$; Fig. 6D–F).

To corroborate the translational relevance of this effect, we established a DOX-inducible *PARP1*-overexpressing stable cell line ($p < 0.01$; Fig. 6G) and employed a subcutaneous xenograft model in nude mice. The *in vivo* experimental results showed that inducing *PARP1* overexpression in combination with niraparib treatment results in significantly greater inhibition of tumor growth compared to treatment with niraparib alone, as evidenced by markedly reduced tumor volume and wet weight ($p < 0.001$; Fig. 6H–J).

Collectively, this study demonstrates that restoring *PARP1* expression can partially reverse the acquired resistance to niraparib both *in vitro* and *in vivo* within the BRCAwt ovarian cancer model. This result not only provides direct evidence confirming *PARP1* as a critical target for niraparib's therapeutic efficacy but also further underscores the key role of its downregulated expression or function in the underlying acquisition and maintenance of resistance to niraparib.

Discussion

This study systematically reveals that the downregulation of *PARP1* expression serves as an important mechanism driving acquired resistance to niraparib in a BRCAwt ovarian cancer preclinical model. Through integrative transcriptomic, proteomic, and systematic *in vitro* and *in vivo* functional experiments, we confirmed the specific downregulation of *PARP1* in resistant cells. This downregulation directly reduces cellular sensitivity to niraparib, whereas restoration of PARP1 expression partially reverses resistance. These findings establish a novel "target diminution" resistance pathway distinct from classical mechanisms such as repair pathway reactivation or drug efflux.

Current research on acquired resistance mechanisms to PARP inhibitors, particularly niraparib, has advanced substantially in patients with HRD, such as those harboring BRCA mutations, where core resistance mechanisms primarily involve restoration of HR function (e.g., BRCA reversion mutations, 53BP1 loss) [4,9,11]. However, in the substantial proportion of BRCAwt/HRD-negative patients, resistance mechanisms exhibit greater complexity and high heterogeneity. The *PARP1* downregulation mechanism identified in this study within a BRCAwt context is fundamentally distinct from the classical HR restoration pathway. This mechanism does not confer resistance by restoring downstream DNA repair capacity, but rather by reducing the initial drug target, thereby weakening its core toxicity (i.e., the PARP trapping effect) at the upstream stage of drug action, providing a novel perspective on resistance mechanisms in this patient population.

As the core molecular target for all clinically used PARP inhibitors, the expression level, functional status, and dynamic behavior of *PARP1* within the DNA damage response network collectively form a complex foundation determining drug efficacy and resistance [14]. Cross-cancer studies, including work by Liu et al. [23] in breast cancer, Gajan et al. [24], and Tsujino et al. [25] in prostate cancer, have confirmed the close association between *PARP1* downregulation and PARP inhibitor resistance. Echoing this, our findings systematically validate, within the BRCAwt ovarian cancer population—where response to PARP inhibitors (especially niraparib) is limited and clinical need is urgent—that *PARP1* downregulation is a key factor driving acquired resistance, thereby directly linking this fundamental biological mechanism to a clear clinical challenge.

The evolution of resistance is a multidimensional dynamic process, extending far beyond simple changes in target protein abundance. Recent research reveals that a series of post-translational modifications profoundly regulate the function and activity of *PARP1*, thereby influencing drug sensitivity. For instance, Zhang et al. [26] discovered that palmitoylation mediated by the palmitoyltransferase *ZDHHC12* negatively regulates the DNA-binding capacity of *PARP1*; inhibiting this modification enhances the efficiency of PARP1 "trapping" by the drug, offering a new target for reversing ovarian cancer resistance. Conversely, research by Chen et al. [27] indicates that FGFR3-induced phosphorylation of *PARP1* at tyrosine 158 (Y158) can promote homologous recombination repair by recruiting *BRG1* and stabilizing *MRE11*, thereby conferring PARP inhibitor resistance to breast cancer cells. Furthermore, Pettitt et al. [28], through large-scale genetic screening, identified various *PARP1* DNA-binding domain mutations that cause resistance; these mutations can directly impair its binding to damaged DNA, rendering the classic "trapping" mechanism ineffective—a finding also corroborated in clinical resistance cases.

Beyond directly affecting its enzymatic activity and DNA-binding properties, *PARP1* also acts as a crucial transcriptional regulatory hub, reshaping cellular states through its non-catalytic functions. Research by Ding et al. [29] reveals that *PARP1* can directly bind to and repress the promoter of *SNAI2*, a key epithelial-mesenchymal transition factor; its loss or inhibition relieves this repression, driving resistance to talazopari. In contrast, a study by Ma et al. [30] reveals that the high-mobility group protein *HMGB3*, by interacting with *PARP1*, promotes its dissociation from damage sites under DNA damage conditions, and its high expression is conversely associated with PARP inhibitor resistance. This highlights the fine-tuning of drug response by

the dynamic balance between *PARP1* and different interacting protein networks.

To better understand resistance, it is necessary to return to the core physiological functions of *PARP1* in maintaining genomic stability. PARP1 is the primary sensor and initiator of DNA single-strand break repair, and the PAR chains it catalyzes are key signals for recruiting downstream repair factors (e.g., *XRCC1*). More importantly, during S phase, *PARP1*, by interacting with replisome proteins (e.g., TIMELESS), plays a protective role in stabilizing replication forks and mitigating "transcription-replication conflicts" [31,32,33]. This challenges the traditional view that PARP inhibitor toxicity stems entirely from "trapping" and the formation of toxic complexes. In fact, recent evidence suggests that the inhibition of *PARP1* enzymatic activity by PARP inhibitors itself, in an HR-deficient context, may be sufficient to trigger synthetic lethality by disrupting fork protection. Therefore, tumor cells may downregulate *PARP1* expression or inactivate its function. While reducing drug "trapping", they might also upregulate other alternative repair pathways (e.g., error-prone microhomology-mediated end joining) or reinforce fork protection mechanisms (e.g., via R-loops), thereby achieving survival through complex adaptive adjustments. Recently, Marks et al. [34] developed an endogenous *PARP1* FRET biosensor based on CRISPR-Cas9, combined with fluorescence lifetime imaging, enabling for the first time real-time, single-cell quantitative analysis of PARP trapping dynamics in living cells. This technology confirms that PARP inhibitor resistance is directly associated with reduced PARP trapping efficiency, providing a powerful tool for understanding resistance at a dynamic level. These studies collectively indicate that the retention kinetics of *PARP1* at DNA damage sites (i.e., trapping) are key to determining efficacy; any factor affecting its binding affinity, post-catalytic dissociation, or protein stability will ultimately alter this kinetic process, leading to resistance.

Although traditional research has focused primarily on the inhibition of *PARP1* enzymatic activity and its "trapping" effect [35], and sporadic reports in recent years have suggested a potential association between *PARP1* expression levels and initial treatment response, systematic functional validation in BRCAwt acquired-resistance models has been lacking [36]. The innovation of our study lies in the use of a long-term induced, homologous recombination-proficient resistance model to demonstrate that *PARP1* downregulation is an active adaptive event during resistance development, rather than merely an epiphenomenon. More importantly, we rigorously established a causal relationship between *PARP1* downregulation and the resistant phenotype through *in vitro* and *in vivo* rescue experiments. This finding aligns with the recently proposed "target loss" resistance paradigm—where tumors evade targeted therapy by reducing target protein levels—thereby adding a crucial component to the current understanding of PARP inhibitor resistance mechanisms.

In addition to *PARP1*, our transcriptomic analysis identified other genes significantly altered in resistant cells, such as the downregulation of *S100A10* and *THBS1*, and the upregulation of *SLC43A3*. These genes are not classical drug efflux pumps; their functions involve calcium signaling, extracellular matrix interaction, and amino acid transport, suggesting that resistance may be accompanied by extensive reprogramming of cell membrane function and microenvironment crosstalk. However, our survival analysis indicated that changes in the expression of these individual genes were not significantly associated with patient prognosis, implying they may be more cooperative or incidental events in the adaptation process rather than independent drivers or prognostic markers. In contrast, the downregulation of the key histone *H2BC8* warrants attention. *H2B* variants are involved in chromatin dynamics, and their alteration may affect DNA damage response efficiency through epigenetic means. Although its direct role in PARPi resistance has not been extensively studied, our finding provides a basis for further exploring the role of chromatin remodeling in resistance.

This study also has several limitations. First, the resistance model was established in a single cell line under constant high-dose selection, which may not fully mirror the gradual clinical evolution of resistance. Validation in additional models, including patient-derived samples, and the use of stepwise dose escalation in future studies are needed. Second, although *PARP1* downregulation drives resistance, its upstream regulatory mechanisms (transcriptional, epigenetic, or post-transcriptional) remain unclear; future studies using ChIP-seq and methylation analyses are needed to address this issue. Third, the marked reduction in PARP1 protein relative to its mRNA decline suggests potential post-translational regulation (e.g., ubiquitination), although the specific mediators remain unknown; future studies using protein stability assays and E3 ligase screens are needed. Finally, the functional state of *PARP1* in resistant cells (activity, trapping capacity) was not directly assessed and warrants further investigation using biochemical and proximity-based assays.

Conclusion

This study demonstrates that, in BRCAwt ovarian cancer, niraparib resistance is accompanied by multi-layered molecular reprogramming, with loss of *PARP1* expression identified as a key mechanism driving resistance. Functional experiments, both *in vitro* and *in vivo*, establish a direct causal relationship between *PARP1* levels and drug sensitivity. These findings enhance our understanding of PARP inhibitor resistance and suggest that targeting pathways regulating *PARP1* expression may offer a novel therapeutic strategy for overcoming resistance.

Availability of Data and Materials

Data generated or analyzed during this study are included in this article, and further datasets are available from the corresponding authors on reasonable request.

Author Contributions

SJC contributed to data visualization and participated in critical data validation. YZL contributed to methodological design and research conceptualization. JYL contributed to data acquisition and analysis. JRL contributed to data analysis and visualization. DZ, TLM, and TTL contributed to data validation. YYT and JLD contributed to the experimental design. MHZ, QSQ, and YQJ contributed to the research direction and experimental design. SJC and YZL have been involved in drafting the manuscript and all authors have been involved in revising it critically for important intellectual content. All authors gave final approval of the version to be published. All authors have participated sufficiently in the work to take public responsibility for appropriate portions of the content and agreed to be accountable for all aspects of the work in ensuring that questions related to its accuracy or integrity.

Ethics Approval and Consent to Participate

The study was approved by the Institutional Animal Care and Use Committee (IACUC) of Huizhou Central People's Hospital (No. GDY2402745). All procedures complied with the ARRIVE Guidelines 2.0.

Acknowledgment

We gratefully acknowledge all colleagues who contributed to and supported this research.

Funding

This study was supported by the Guangdong Basic and Applied Basic Research Foundation (2023B1515120085, 2024A1515110272 and 2022A1515110197), the Shenzhen Science and Technology Program (JCYJ20220530152008019) and Huizhou Science and Technology Program (2024CZ010270).

Conflict of Interest

The authors declare no conflict of interest.

Supplementary Material

Supplementary material associated with this article can be found, in the online version, at https://doi.org/10.24976/Discov.Med.202638210.179.

References

[1] O'Malley DM, Krivak TC, Kabil N, Munley J, Moore KN. PARP Inhibitors in Ovarian Cancer: A Review. Targeted Oncology. 2023; 18: 471–503. https://doi.org/10.1007/s11523-023-00970-w

[2] Xie T, Dickson KA, Yee C, Ma Y, Ford CE, Bowden NA, et al. Targeting Homologous Recombination Deficiency in Ovarian Cancer with PARP Inhibitors: Synthetic Lethal Strategies That Impact Overall Survival. Cancers. 2022; 14: 4621. https://doi.org/10.3390/cancers14194621

[3] Chandrasekaran A, Elias KM. Synthetic Lethality in Ovarian Cancer. Molecular Cancer Therapeutics. 2021; 20: 2117–2128. https://doi.org/10.1158/1535-7163.MCT-21-0500

[4] Akay M, Funingana IG, Patel G, Mustapha R, Gjafa E, Ng T, et al. An In-Depth Review of Niraparib in Ovarian Cancer: Mechanism of Action, Clinical Efficacy and Future Directions. Oncology and Therapy. 2021; 9: 347–364. https://doi.org/10.1007/s40487-021-00167-z

[5] Monk BJ, Barretina-Ginesta MP, Pothuri B, Vergote I, Graybill W, Mirza MR, et al. Niraparib first-line maintenance therapy in patients with newly diagnosed advanced ovarian cancer: final overall survival results from the PRIMA/ENGOT-OV26/GOG-3012 trial. Annals of Oncology : Official Journal of the European Society for Medical Oncology. 2024; 35: 981–992. https://doi.org/10.1016/j.annonc.2024.08.2241

[6] Purwar R, Ranjan R, Pal M, Upadhyay SK, Kumar T, Pandey M. Role of PARP inhibitors beyond BRCA mutation and platinum sensitivity in epithelial ovarian cancer: a meta-analysis of hazard ratios from randomized clinical trials. World Journal of Surgical Oncology. 2023; 21: 157. https://doi.org/10.1186/s12957-023-03027-4

[7] Bonadio RC, Estevez-Diz MDP. Perspectives on PARP Inhibitor Combinations for Ovarian Cancer. Frontiers in Oncology. 2021; 11: 754524. https://doi.org/10.3389/fonc.2021.754524

[8] Coleman RL, Perhanidis JA, Kalilani L, Zimmerman NM, Golembesky A, Moore KN. Real-world overall survival in second-line maintenance niraparib monotherapy versus active surveillance in patients with *BRCA* wild-type recurrent ovarian cancer. Therapeutic Advances in Medical Oncology. 2024; 16: 17588359241292272. https://doi.org/10.1177/17588359241292272

[9] Apelian S, Martincuks A, Whittum M, Yasukawa M, Nguy L, Mathyk B, et al. PARP Inhibitors in Ovarian Cancer: Resistance Mechanisms, Clinical Evidence, and Evolving Strategies. Biomedicines. 2025; 13: 1126. https://doi.org/10.3390/biomedicines13051126

[10] Kyo S, Kanno K, Takakura M, Yamashita H, Ishikawa M, Ishibashi T, et al. Clinical Landscape of PARP Inhibitors in Ovarian Cancer: Molecular Mechanisms and Clues to Overcome Resistance. Cancers. 2022; 14: 2504. https://doi.org/10.3390/cancers14102504

[11] Zou Y, Zhang H, Chen P, Tang J, Yang S, Nicot C, et al. Clinical approaches to overcome PARP inhibitor resistance. Molecular Cancer. 2025; 24: 156. https://doi.org/10.1186/s12943-025-02355-1

[12] Xu L, Kong X, Zhang B, Ma H, Li X, Deng Y, et al. Interplay Between Poly(ADP-ribosyl)ation and Specific Inner Cellular Events That Suggest Combination Strategies for Overcoming PARP Inhibitor Resistance. Pharmaceutics. 2026; 18: 355. https://doi.org/10.3390/pharmaceutics18030355

[13] Liu C, Li J, Xu F, Chen L, Ni M, Wu J, et al. PARP1-DOT1L transcription axis drives acquired resistance to PARP inhibitor in ovarian cancer. Molecular Cancer. 2024; 23: 111. https://doi.org/10.1186/s12943-024-02025-8

[14] Kanev PB, Atemin A, Stoynov S, Aleksandrov R. PARP1 roles in DNA repair and DNA replication: The basi(c)s of PARP in-

hibitor efficacy and resistance. Seminars in Oncology. 2024; 51: 2–18. https://doi.org/10.1053/j.seminoncol.2023.08.001

[15] Jiang X, Li X, Li W, Bai H, Zhang Z. PARP inhibitors in ovarian cancer: Sensitivity prediction and resistance mechanisms. Journal of Cellular and Molecular Medicine. 2019; 23: 2303–2313. https://doi.org/10.1111/jcmm.14133

[16] Lee EK, Matulonis UA. PARP Inhibitor Resistance Mechanisms and Implications for Post-Progression Combination Therapies. Cancers. 2020; 12: 2054. https://doi.org/10.3390/cancers12082054

[17] Lin H, Jin HY, Lyu WG. Metabolic signatures of niraparib-resistant ovarian cancer cells based on non-target metabolomics. Zhonghua Fu Chan Ke Za Zhi. 2025; 60: 608–616. https://doi.org/10.3760/cma.j.cn112141-20250113-00023 (In Chinese)

[18] Wang M, Yuan C, Wu Z, Xu M, Chen Z, Yao J, et al. Paris saponin VII reverses resistance to PARP inhibitors by regulating ovarian cancer tumor angiogenesis and glycolysis through the RORα/ECM1/VEGFR2 signaling axis. International Journal of Biological Sciences. 2024; 20: 2454–2475. https://doi.org/10.7150/ijbs.91861

[19] van Beek L, McClay É, Patel S, Schimpl M, Spagnolo L, Maia de Oliveira T. PARP Power: A Structural Perspective on PARP1, PARP2, and PARP3 in DNA Damage Repair and Nucleosome Remodelling. International Journal of Molecular Sciences. 2021; 22: 5112. https://doi.org/10.3390/ijms22105112

[20] Thorsell AG, Ekblad T, Karlberg T, Löw M, Pinto AF, Trésaugues L, et al. Structural Basis for Potency and Promiscuity in Poly(ADP-ribose) Polymerase (PARP) and Tankyrase Inhibitors. Journal of Medicinal Chemistry. 2017; 60: 1262–1271. https://doi.org/10.1021/acs.jmedchem.6b00990

[21] Jones P, Altamura S, Boueres J, Ferrigno F, Fonsi M, Giomini C, et al. Discovery of 2-{4-[(3S)-piperidin-3-yl]phenyl}-2H-indazole-7-carboxamide (MK-4827): a novel oral poly(ADP-ribose)polymerase (PARP) inhibitor efficacious in BRCA-1 and -2 mutant tumors. Journal of Medicinal Chemistry. 2009; 52: 7170–7185. https://doi.org/10.1021/jm901188v

[22] Lindgren AEG, Karlberg T, Thorsell AG, Hesse M, Spjut S, Ekblad T, et al. PARP inhibitor with selectivity toward ADP-ribosyltransferase ARTD3/PARP3. ACS Chemical Biology. 2013; 8: 1698–1703. https://doi.org/10.1021/cb4002014

[23] Liu X, Han EK, Anderson M, Shi Y, Semizarov D, Wang G, et al. Acquired resistance to combination treatment with temozolomide and ABT-888 is mediated by both base excision repair and homologous recombination DNA repair pathways. Molecular Cancer Research : MCR. 2009; 7: 1686–1692. https://doi.org/10.1158/1541-7786.MCR-09-0299

[24] Gajan A, Sarma A, Kim S, Gurdziel K, Wu GS, Shekhar MP. Analysis of Adaptive Olaparib Resistance Effects on Cisplatin Sensitivity in Triple Negative Breast Cancer Cells. Frontiers in Oncology. 2021; 11: 694793. https://doi.org/10.3389/fonc.2021.694793

[25] Tsujino T, Takai T, Hinohara K, Gui F, Tsutsumi T, Bai X, et al. CRISPR screens reveal genetic determinants of PARP inhibitor sensitivity and resistance in prostate cancer. Nature Communications. 2023; 14: 252. https://doi.org/10.1038/s41467-023-35880-y

[26] Zhang X, Liu Y, Liao X, Wang M, Liu J, Wen Y, et al. Targeting ZDHHC12-mediated PARP1 palmitoylation potentiates PARP inhibitor cytotoxicity. Cell Reports. 2026; 45: 116910. https://doi.org/10.1016/j.celrep.2025.116910

[27] Chen MK, Yamaguchi H, Gao Y, Xia W, Chang JT, Hsiao YC, et al. FGFR3-induced Y158 PARP1 phosphorylation promotes PARP inhibitor resistance via BRG1/MRE11-mediated DNA repair in breast cancer models. The Journal of Clinical Investigation. 2025; 135: e173757. https://doi.org/10.1172/JCI173757

[28] Pettitt SJ, Krastev DB, Brandsma I, Dréan A, Song F, Aleksandrov R, et al. Genome-wide and high-density CRISPR-Cas9 screens identify point mutations in PARP1 causing PARP inhibitor resistance. Nature Communications. 2018; 9: 1849. https://doi.org/10.1038/s41467-018-03917-2

[29] Ding X, Zhu Z, Lapek J, McMillan EA, Zhang A, Chung CY, et al. PARP1-SNAI2 transcription axis drives resistance to PARP inhibitor, Talazoparib. Scientific Reports. 2022; 12: 12501. https://doi.org/10.1038/s41598-022-16623-3

[30] Ma H, Qi G, Han F, Lu W, Peng J, Li R, et al. HMGB3 promotes PARP inhibitor resistance through interacting with PARP1 in ovarian cancer. Cell Death & Disease. 2022; 13: 263. https://doi.org/10.1038/s41419-022-04670-7

[31] Saldanha J, Rageul J, Patel JA, Phi AL, Lo N, Park JJ, et al. The TIMELESS and PARP1 interaction suppresses replication-associated DNA gap accumulation. Nucleic Acids Research. 2024; 52: 6424–6440. https://doi.org/10.1093/nar/gkae445

[32] Rageul J, Lo N, Phi AL, Patel JA, Park JJ, Kim H. Poly(ADP-ribosyl)ation of TIMELESS limits DNA replication stress and promotes stalled fork protection. Cell Reports. 2024; 43: 113845. https://doi.org/10.1016/j.celrep.2024.113845

[33] Young LM, Marzio A, Perez-Duran P, Reid DA, Meredith DN, Roberti D, et al. TIMELESS Forms a Complex with PARP1 Distinct from Its Complex with TIPIN and Plays a Role in the DNA Damage Response. Cell Reports. 2015; 13: 451–459. https://doi.org/10.1016/j.celrep.2015.09.017

[34] Marks D, Garcia E, Kumar S, Tyson K, Koch C, Ivanov AP, et al. Assessing PARP trapping dynamics in ovarian cancer using a CRISPR-engineered FRET biosensor. Cell Reports Methods. 2026; 6: 101270. https://doi.org/10.1016/j.crmeth.2025.101270

[35] Murai J, Huang SYN, Das BB, Renaud A, Zhang Y, Doroshow JH, et al. Trapping of PARP1 and PARP2 by Clinical PARP Inhibitors. Cancer Research. 2012; 72: 5588–5599. https://doi.org/10.1158/0008-5472.CAN-12-2753

[36] Gogola E, Duarte AA, de Ruiter JR, Wiegant WW, Schmid JA, de Bruijn R, et al. Selective Loss of PARG Restores PARylation and Counteracts PARP Inhibitor-Mediated Synthetic Lethality. Cancer Cell. 2018; 33: 1078–1093.e12. https://doi.org/10.1016/j.ccell.2018.05.008